ZCS Resonant Converter Based Parallel Balancing of Serially Connected Batteries String

Ilya Zeltser, *Member, IEEE*

Power Electronics Department
Rafael Advanced Defense Systems Ltd.
P.O. Box 2250, Haifa 31021, Israel.
ilyaz@rafael.co.il
www.rafael.co.il

Or Kirshenboim, *Student Member, IEEE*, Nadav Dahan, *Student Member, IEEE*, and Mor Mordechai Peretz, *Member, IEEE*

The Center for Power Electronics and Mixed-Signal IC
Department of Electrical and Computer Engineering
Ben-Gurion University of the Negev
P.O. Box 653, Beer-Sheva 84105, Israel.
orkir@post.bgu.ac.il, nadad@post.bgu.ac.il,
morp@ee.bgu.ac.il
www.ee.bgu.ac.il/~pemic

***Abstract* – This paper introduces a new topology for parallel balancing of serially connected batteries string. The main advantage of the balancing concept is that energy is transferred only when the cells are unbalanced. As a result, the power losses are significantly reduced since no current circulates through the system when balanced. This has been enabled by a modification of an isolated series-resonant converter operating in DCM and features zero current switching (ZCS). Another attractive feature is that one transformer for two cells is used, as opposed to conventional isolated topologies that require a transformer per cell. The realization is simple and requires simple current polarity detector. Experimental results have been obtained by a prototype of two series connected batteries, which demonstrates the balancing capabilities of the system.**

I. Introduction

Serially connected batteries strings have been used for many high voltage DC applications. Among them, electric vehicles (EV) [1], hybrid electric vehicles (HEV) [2], plug-in hybrid electric vehicle (PHEV) [3] and other battery powered applications [4], [5]. Due to manufacturing and environmental variances, degradation with aging, internal impedance difference and thermal conditions, the charges transferred to or consumed from each battery are not equal. As a result, the lifetime and efficiency of the batteries string are reduced. Moreover, the overcharge of the batteries in the string can cause explosion or fire in the case of sensitive batteries cells [6]. Therefore, a charge equalizer (i.e., balancing circuit) is essential to reduce the imbalances and consequently to improve the overall performance of the system [7], [8].

Several balancing circuits have been investigated over the recent years [9]-[33]. These can be generally classified into two main categories: passive and active. Passive balancing features simple design and implementation and relatively low cost [9], but due to inherent energy loss, it is less attractive in terms of energy saving. The active balancing architectures include variety of topologies such as switched-capacitor converters [10]-[12], isolated and non-isolated unidirectional and bidirectional DC-DC converters [13]-[24], and multi-winding transformer-based converters [25]-[27]. The main challenges of the active solutions often relate to implementation issues such as high component count and complex control algorithms [28], [29]. In addition, increasing the balancing speed is traded for quiescent power loss, i.e. losses that exist when no balancing action is required.

Recent studies have reported improved balancing schemes that are based on parallel balancing techniques [30], exhibiting higher equalization speed when compared to series balancing techniques. One particular challenge of the parallel balancing is the complexity in implementing large arrays. This has been addressed by a modularization concept presented in [31]-[34]. There, n batteries string is divided into M modules, each of them is balancing K cells so that $n=M*K$. This concept has established a solid foundation for a parallel balancing architecture, allowing higher efficiency that is pursued in this study.

The objective of the study is to introduce a new active balancing converter topology for series connected batteries string, as detailed in Fig. 1. The concept is realized by a modification of an isolated series-resonant converter such that one transformer is used to balance two cells, reducing the complexity of the system. The converter operates in DCM and therefore ZCS is assured. Balancing occurs only when necessary, i.e. energy does not circulate through the system when the batteries are balanced. As a result, the quiescent power loss is minimal. The converter is controlled by simple control method and can be easily scaled up and modularized.

978-1-4673-9550-2/16/$31.00 ©2016 IEEE

The paper is organized as follows: Section II describes the topology, its principle of operation and the major features of it, Section III delineates the system's implementation and provides design guidelines. Experimental results and conclusion are then provided in Sections IV and V, respectively.

II. Principle of Operation

The system in Fig. 1 can be divided into $m = n/2$ double-cell modules, where each module is constructed of a top cell (odd-numbered cells) and a bottom cell (even-numbered cells). Each of the m double-cells is balanced using a balancing module, built of a half-bridge loaded by a resonant tank in series with the primary side of the transformer. The secondary side connects to the bus capacitor via a full-bridge transistor assembly. The bus capacitor is the common voltage for all of the m double-cell modules and acts as a "link" that is used to transfer energy between the cells. As a result of the transformer's isolation, each of the n battery cells can be equalized independently of the action in other cells, that is, no synchronization between the modules is required, and therefore the complexity of the system is significantly reduced. Additionally, due to the transformer's isolation, the voltage stress on the switches is no more than the cell voltage and is independent on the number of cells in the string. The switching frequency f_s is set to be lower than the resonant frequency f_r (i.e. $f_s<f_r$) to allow operation in DCM with ZCS.

The balancing action for each battery cell is divided into two steps: current polarity detection and then directional energy transfer based on the polarity. The operation of the switches is described in Fig. 2 for the upper cell, assisted by the current and voltage waveforms which are depicted in Fig. 3. In the first step, switches S_{m1}, S_{m3}, S_{m5} and S_{m8} are turned on at $t=t_0$, and remain on for $t_0<t<t_1$ ((Fig. 2(a), Fig. 2(d)), where $t_1<t_0+1/2f_r$, allowing bi-directional current flow. During this interval, the current polarity sensor determines the current direction in the resonant tank. The current direction depends on the difference between the battery cell voltage $V_{cell,n-1}$ and the bus voltage reflected to the primary (V_{bus} for the unity transformer ratio). Cell voltage that is higher than twice the bus capacitor voltage ($V_{cell,n-1}>2V_{bus}$) results in a positive current i_r, whereas $V_{cell,n-1}<2V_{bus}$, results in a negative current direction. In case that the cell voltage equals twice the bus capacitor voltage ($V_{cell,n-1}=2V_{bus}$), i.e., no balancing is needed, the current is zero and no energy is transferred in either direction. The current polarity is detected by a sensor at the primary side, as shown in Fig. 2(a) and in Fig. 2(d), that determines the consecutive switching sequence in the second step. It should be noted that the switching configuration at the beginning of the switching cycle ($t_0<t<t_1$) is similar regardless of the difference between the cell and the bus voltages, that is for both positive and negative current.

In the second step, after the current polarity has been detected, the operation resembles a conventional resonant converter in DCM. For positive detected current, S_{m5} and S_{m8} turn off at t_1, and their body diodes are conducting until the current becomes zero at $t=t_0+1/2f_r$ (Fig. 2(b)). It should be noted that turning S_{m5} and S_{m8} off at a low, nonzero current (before t_1) further allows ZVS at turn off. The current remains zero until half of the switching period $t_2=t_0+1/2f_s$. At t_2, S_{m1} turns off and, followed by a short dead-time, S_{m2} turns on (Fig. 2(c)). This discharges the resonant capacitor with a negative current during $t_2<t<t_2+1/2f_r$ and then the current is discontinued by the body diodes of S_{m6} and S_{m7} until the next switching cycle at $t_3=t_0+1/f_s$.

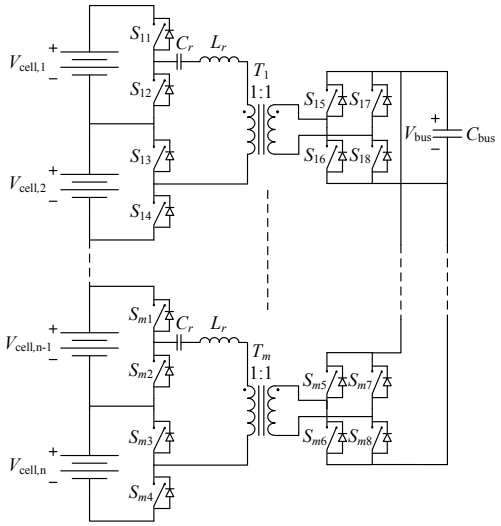

Fig. 1. Battery management system for n serially connected batteries.

For a negative detected current at $t_0<t<t_1$, the operation is mirrored with respect to the cell and the bus side. S_{m1} is turned off at t_1, as shown in Fig. 2(e). The switches S_{m5}, S_{m8} are turned off and S_{m6}, S_{m7} are turned on (after a short dead-time) at t_2 (Fig. 2(f)). It should be noted that the switching timing can be loosely set. ZCS is naturally obtained by the body diodes as long as the switches have been turned off prior to the zero crossing point [35].

Simulated typical convergence during balancing operation of the system is presented in Fig. 4, where four battery cells (emulated by large capacitances) have been preset to different voltages. As can be observed, the cells voltages converge to the average of the initial voltages, validating the balancing operation of the system. The bus voltage converges to the average of half the voltage levels of the cells in the pack, and is given by

$$V_{bus} = \frac{1}{2N}\sum_{k=1}^{N} V_{cell,k} \tag{1}$$

To derive the expressions for the system's key waveforms and parameters, in the following analysis, it is assumed that the cell voltage (V_{cell}) and the bus voltage V_{bus} are constant and that the average voltage across the resonant capacitor has reached a

steady-state value of half the cell voltage, i.e. V_{Cr}=0.5V_{cell}. It is further assumed that the charge capacity of the bus capacitor is significantly lower than the cells' capacity. As a result, the bus voltage rapidly converges to the half of the average cells' voltages as in (1) which translates to a relatively small voltage difference ΔV=0.5V_{cell}-V_{bus} during steady-state. Due to symmetrical operation, the derivations are applied for the case that V_{cell}>2V_{bus}. The resonant current i_r can be expressed as

$$i_r(t)=\begin{cases}\dfrac{0.5V_{cell}-V_{bus}}{\left(1-e^{-\frac{\pi}{4Q}}\right)Z_r}e^{-\frac{2\pi f_r}{2Q}t}\sin(2\pi f_r t) & ,\ t_0\le t\le t_0+1/2f_r\\ -\dfrac{0.5V_{cell}-V_{bus}}{\left(1-e^{-\frac{\pi}{4Q}}\right)Z_r}e^{-\frac{2\pi f_r}{2Q}t}\sin(2\pi f_r t) & ,\ t_2\le t\le t_2+1/2f_r\\ 0 & ,\ \text{elsewhere}\end{cases} \quad (2)$$

where, the resonant tank's characteristic impedance Z_r, resonant frequency f_r and the quality factor Q are:

$$Z_r=\sqrt{\frac{L_r}{C_r}};\ f_r=\frac{1}{2\pi\sqrt{L_rC_r}};\ Q=\frac{1}{R}\sqrt{\frac{L_r}{C_r}} \quad (3)$$

and, L_r and C_r are the resonant network components and R is the total parasitic or stray series resistance in the resonant network.

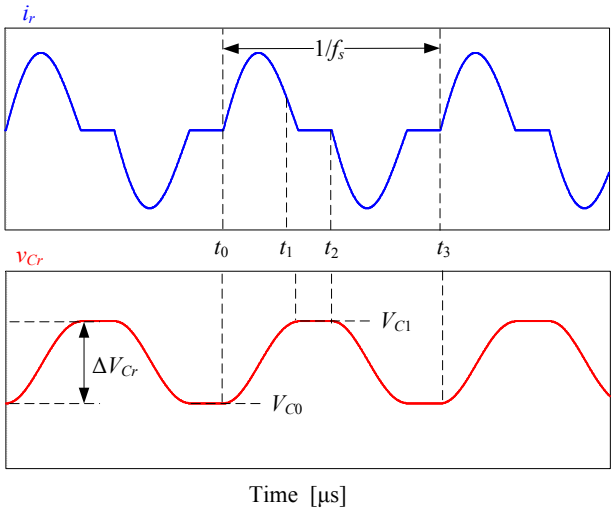

Fig. 3. Typical waveforms of the resonant inductor current and resonant capacitor voltage during balancing for the case when $V_{cell,n-1}$>2V_{bus}.

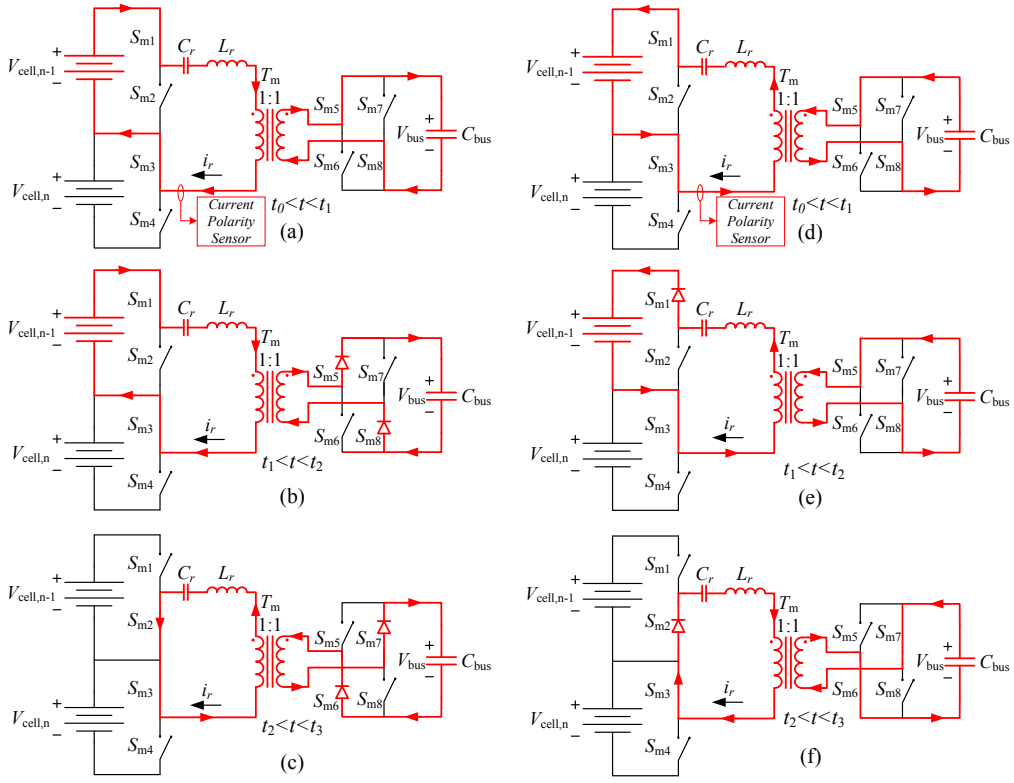

Fig. 2. Modes of operation: (a), (b) and (c) when $V_{cell,n-1}$>2V_{bus}, (d), (e) and (f) when $V_{cell,n-1}$<2V_{bus}. (a) and (d): current polarity detection at $t_0<t<t_1$, (b), (c), (e) and (f): energy transfer.

From (2), the peak amplitude of the resonant current and the average current flowing through the cell can be expressed as:

$$I_{\text{peak}} = \frac{0.5V_{\text{cell}} - V_{\text{bus}}}{Z_r} \frac{e^{-\frac{\pi}{4Q}}}{1-e^{-\frac{\pi}{4Q}}}, \tag{4}$$

$$I_{\text{cell}} = \frac{\delta}{\pi} I_{\text{peak}} = \frac{\delta}{\pi} \frac{0.5V_{\text{cell}} - V_{\text{bus}}}{Z_r} \frac{e^{-\frac{\pi}{4Q}}}{1-e^{-\frac{\pi}{4Q}}}, \tag{5}$$

where $\delta=0.5f_s/f_r$. The voltage swing of the resonant capacitor ΔV_{Cr} during one switching cycle $T_s=1/f_s$ can be expressed as:

$$\Delta V_{C_r} = 2I_{\text{peak}} Z_r \tag{6}$$

where, V_{C0} and V_{C1} are the initial and final voltages (Fig. 3), respectively, given by:

$$\begin{aligned} V_{C_0} &= 0.5(V_{\text{cell}} - \Delta V_{C_r}) \\ V_{C_1} &= 0.5(V_{\text{cell}} + \Delta V_{C_r}) \end{aligned}. \tag{7}$$

The power processing efficiency for a given voltage difference of ΔV can be expressed as:

$$\eta = 1 - \frac{P_{\text{loss}}}{P_{\text{cell}}} = 1 - \frac{\pi}{2} \frac{I_{\text{peak}} Z_r}{V_{\text{cell}} Q} = 1 - \frac{\pi}{2} \frac{\Delta V}{V_{\text{cell}}} \frac{e^{-\frac{\pi}{4Q}}}{1-e^{-\frac{\pi}{4Q}}} \frac{1}{Q}. \tag{8}$$

As mentioned earlier and expresses by (1), the bus voltage converges to half of the cells average voltage. This process can be assumed instantaneous when compared to the rate that cells' voltages vary. As can be seen in (8), the power processing efficiency linearly depends on ΔV, which reflects on the voltage difference between the cells. This implies when balance is achieved the converter exhibits ideal power processing efficiency, a consequence of the fact that no current circulates through the system when balanced. It should be further noted that for a reasonable setting of the resonant parameters of $Q>4$, (8) can be approximated to:

$$\eta = 1 - \frac{\pi}{2} \frac{\Delta V}{V_{\text{cell}}} 1.273, \tag{9}$$

which highlights that the efficiency depends primarily on the cells' status and is virtually independent on the system parameters. A clear advantage in a balancing system or any system that comprises multiple converters or converters string.

III. Implementation, Design Considerations and Topology Expansion

Implementation of each of the m modules in Fig. 1 is straightforward and is depicted in Fig. 5. The battery cell side is built around a conventional resonant half-bridge

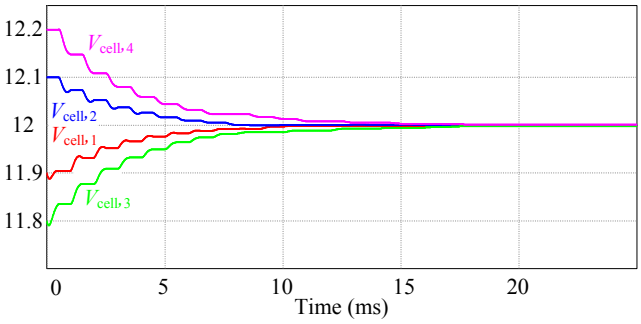

Fig. 4. Simulated convergence of cells with different initial voltage preset.

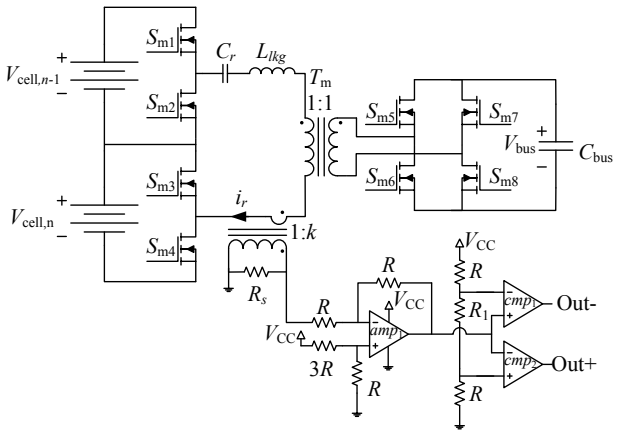

Fig. 5. Implementation of each of the m balancing circuits including the current polarity detection circuitry.

configuration whereas the bus capacitor side is constructed by a standard full-bridge rectifier configuration. As a result, the design of the MOSFET's gates drivers is standard low-side and bootstrapped pairs. The design of the resonant inductance and transformer follows a classical LLC magnetic element design, where L_r can be the leakage inductance L_{lkg} of the transformer which has been estimated as described in [36].

A. Design Considerations

The analysis derived earlier established the main attributes of the converter. Utilizing the above derivations, calculations of the key components of the converter can be established by the following procedure.

Given: Target average current per cell I_{cell} for maximum setting of ΔV; the switching frequency f_s and quality factor $Q>4$.

a. Calculate the expression

$$F(Q) = \frac{e^{-\frac{\pi}{4Q}}}{1-e^{-\frac{\pi}{4Q}}} \tag{10}$$

b. From (5), (10), and considering $\delta < 1/2$, L_r and C_r can be selected according to

$$L_r < \frac{F(Q)\Delta V}{(2\pi)^2 I_{\text{cell}} f_s} \tag{11}$$

$$\left(\frac{2\pi I_{\text{cell}}}{F(Q)\Delta V}\right)^2 L_r < C_r < \left(\frac{1}{2\pi f_s}\right)^2 \frac{1}{L_r} \tag{12}$$

c. Verify that the resonant tank's series resistance R satisfies

$$R < \frac{Z_r}{Q} \ . \tag{13}$$

If (13) does not hold, iterate (11) and (12).

d. The transformer's area of product $A_p^{'}$ (without the leakage inductance consideration) should be selected according to

$$A_p' > \frac{V_{\text{bus}} I_{\text{peak}}}{\Delta B J K} \sqrt{\frac{f_r}{2 f_s}} \tag{14}$$

where ΔB is the magnetic flux density at saturation, J is the current density and K is the winding fill factor.

e. To achieve the desired leakage inductance L_{lkg} the transformer's windings configuration should be designed as illustrated in Fig. 6 (for an E-type magnetic core). As prescribed in [36], the leakage inductance in E core can be estimated by

$$L_{lkg} = \frac{\mu_0 n^2 ATL}{a}\left(\frac{b_1 + b_2}{3} + c\right)[H], \tag{15}$$

where μ_0 is the permeability constant, n is the number of turns in the primary winding, ATL is the average length of turn, a is the winding height, b_1 and b_2 are the thicknesses of the primary and secondary winding, respectively, and c is the distance between the primary and the secondary winding. All lengths are assigned in mm.

In this study, the transformer is with a 1:1 turns ratio and therefore $b_1=b_2=b$.

f. Adjust the area product to include the addition of the leakage inductance by

$$A_p = A_p'\left(1 + \frac{c}{2b}\right). \tag{16}$$

B. Practical implementation

The current polarity detector circuitry (Fig. 5) is realized using a current transformer, summing amplifier and two comparators, as depicted in Fig. 5. Three operation modes are detected – positive, negative and zero current. The current is

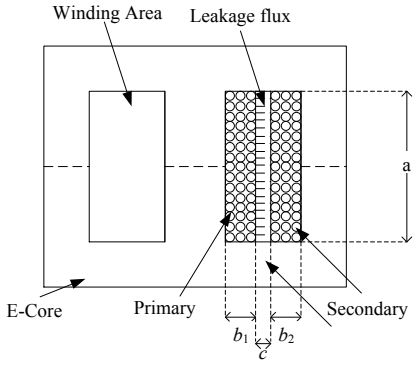

Fig. 6. Conventional transformer winding configuration for an E-core.

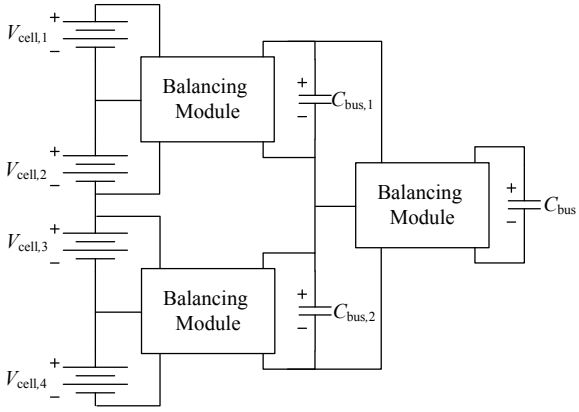

Fig. 7. Modularization of the balancing system for four battery cells.

considered zero if its absolute maximum value, measured within $t_0<t<t_1$, is less than the threshold determined by the following expression:

$$|I_{th}| = \frac{0.5 V_{CC}}{1+2d}\frac{k}{R_s}, \tag{17}$$

where $d=R/R_1$, k is the turns ratio of the current transformer, R_s is the sense resistor at the secondary side of the current transformer, $R>>R_s$, and $R>R_1$. The outputs of the comparators determine the polarity of i_r as detailed in Table I.

TABLE I – CURRENT POLARITY SENSOR DETECTION

Out+	***Out-***	***Current Polarity***
1	0	$i_r > 0$
0	1	$i_r < 0$
0	0	$i_r \approx 0$

The voltage stress of the transistors is the cell voltage for the cell side transistors and the bus capacitor voltage for the bus side. The lower voltage stress allows transistors with lower $R_{\text{DS(on)}}$ per silicon area. Current stresses depend on the desired convergence speed.

The isolation between the bus capacitor and the battery cells provided by the transformer enables the topology to be extended, as demonstrated in Fig. 7, for four battery cells. This modularization, as mentioned in [31], provides another stage of balancing and enables the operation at lower voltage stress which can expedite the balancing speed since higher current can be delivered for the same power dissipation.

IV. Experimental Verification

In order to demonstrate the balancing action and to verify the analysis and simulation results, experiments have been carried out using two large capacitors (emulating the batteries operation, in order to shorten the convergence time) as two cells in series. Table II shows the component types and values used in the experimental prototype. Fig. 8 presents the measured waveforms of the resonant tank during the balancing operation. Based on the principle of operation described earlier, the balancing time is shared equally between the cells. The duration of each cell-balancing has been set to 10 switching cycles. The procedure is demonstrated in Fig. 9, where the resonant current and the capacitor voltage are measured over 20 switching cycle. During the first 10 switching cycles the cell having the higher voltage is balanced (i.e. connects to the bus via the converter), whereas in the next 10 switching cycles the balancing is done for the cell with lower voltage. Convergence of the resonant capacitor voltage to the steady-state value can be observed in Fig. 9, supporting the analysis conjecture that the majority of energy transfer operation is carried under steady-state conditions.

Fig. 10 shows the cells' (realized by large capacitors to allow timely convergence) voltages and the tank's resonant current over a long period of time when cells are pre-charged to different voltages. As can be observed, the voltages of the two cells are equalized one to another and the current decay to zero.

Similar experiment was carried out using two 12 V, 7Ah, Lead-Acid batteries. Fig. 11 shows the batteries voltages over a long period of time when pre-charged to different voltages. As can be observed, the voltages of the two batteries are being balanced up to a small voltage difference.

TABLE II – Experimental Prototype Values

Component	*Value*
Cells: Batteries	12 V, 7Ah
When realized by capacitors	100 mF
Transformer's leakage inductance L_{lkg}	5 µH
Resonant tank capacitor C_r	5.7 µF
Transformer's magnetizing inductance L_m	3 mH
MOSFETs S_{m1}-S_{m8}	Si4178DY
Bus capacitor C_{bus}	15 mF
Resonant frequency f_r	30 kHz
Switching frequency f_s	20 kHz

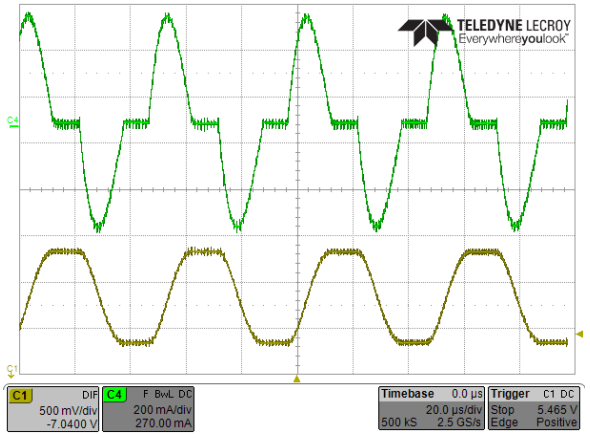

Fig. 8. Experimental results of resonant tank current (top) and resonant capacitor voltage (bottom) during balancing operation. Current 200mA/div, voltage 500mV/div, time scale 20µs/div.

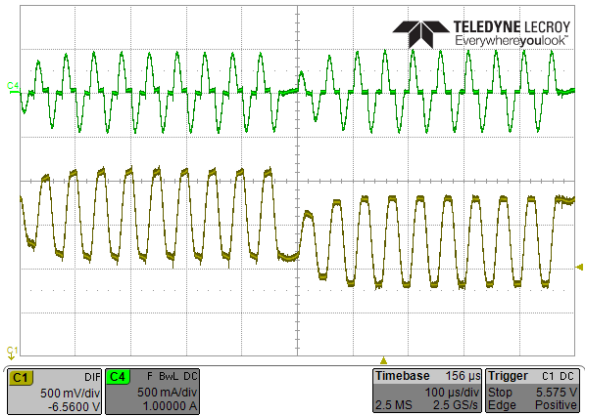

Fig. 9. Resonant tank current (top) and resonant capacitor voltage (bottom) during balancing of upper and lower cells with different voltages, each of them is balanced for 10 switching periods. Current 500mA/div, voltage 500mV/div, time scale 100µs/div.

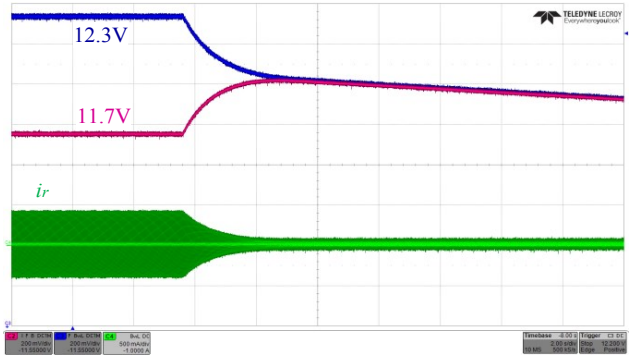

Fig. 10. Experimental results of voltage convergence of two cells with different initial voltages, and the tank's resonant current. Time scale 2s/div, Cells voltages 200mV/div, tank's resonant current 500mA/div.

V. Conclusion

In this work, a new soft switched isolated balancing topology and operation method have been introduced. The circuit is based on a modified series resonant converter operating in DCM. The new balancing circuit uses one transformer for balancing of two neighboring cells and as a result, less magnetic components are required compared to other isolated topologies. Another significant advantage of the topology is the extremely low quiescent losses due to the native behavior of the converter where no current circulates through the system when the cells are balanced.

The balancing operation is facilitated by a simple current polarity detection and does not require synchronization between modules. Furthermore, the topology can be easily scaled-up and modularized for as many cells as required.

Acknowledgements

This research was supported by 'Keren Pazi'.

References

[1] A. Emadi, L. Young Joo, and K. Rajashekara, "Power electronics and motor drives in electric, hybrid electric, and plug-in hybrid electric vehicles," *IEEE Trans. Ind. Electron.*, vol. 55, no. 6, pp. 2237–2245, Jun. 2008.

[2] M. Ehsani, G. Yimin, J. M. Miller, "Hybrid electric vehicles: architecture and motor drives," *Proceedings of the IEEE*, vol. 95, no. 4, pp. 719-728, Apr. 2007.

[3] A. Y. Saber and G. K. Venayagamoorthy, "Plug-in vehicles and renewable energy sources for cost and emission reductions," *IEEE Trans. Ind. Electron.*, vol. 58, no. 4, pp. 1229–1238, Apr. 2011.

[4] H. Qian, J. Zhang, J. S. Lai, and W. Yu, "A high-efficiency grid-tie battery energy storage system," *IEEE Trans. Power Electron.*, vol. 26, no. 3, pp. 886–896, Mar. 2011.

[5] B. Gu, J. Dominic, B. Chen, and J. S. Lai, "A high-efficiency single-phase bidirectional AC-DC converter with minimized common mode voltages for battery energy storage systems," in *Proc. IEEE Energy Convers. Congr. Expo. 2013*, pp. 5145-5149, Sep. 2013.

[6] B. T. Kuhn, G. E. Pitel, and P. T. Krein, "Electrical properties and equalization of lithium-ion cells in automotive applications," in *Proc. IEEE Vehicle Power Propuls. Conf.*, pp. 55–59, Sep. 2005.

[7] P. T. Krein and R. S. Balog, "Life extension through charge equalization of lead–acid batteries," in *Proc. Int. Telecommun. Energy Conf. (INTELEC)*, pp. 516–523, 2002.

[8] M. Uno and K. Tanaka, "Influence of high-frequency charge–discharge cycling induced by cell voltage equalizers on the life performance of lithium-ion cells," *IEEE Trans. Veh. Technol.*, vol. 60, no. 4, pp. 1505–1515, May 2011.

[9] J. Cao, M. Schofield and A. Emadi, "Battery balancing methods: A comprehensive review," *IEEE Vehicle Power and Propulsion Conference, VPPC '08*. pp.1,6, Sep. 2008.

[10] A. C. Baughman and M. Ferdowsi, "Double-tiered switched-capacitor battery charge equalization technique," *IEEE Trans. Ind. Electron.* , vol. 55, no. 6, pp. 2277-2285, Jun. 2008.

[11] C. Pascual and P. T. Krein, "Switched capacitor system for automatic series battery equalization" in *Proc. IEEE Appl. Power Electron. Conf. Expo. 1997*, pp. 848-854, Feb. 1997.

[12] M. W. Cheng, Y. S. Lee, R. H. Chen, and W. T. Sie, "Cell voltage equalization using ZCS SC bidirectional converters," in *Proc. Int. Telecommun. Energy Conf.*, pp. 1–6, Oct. 2009.

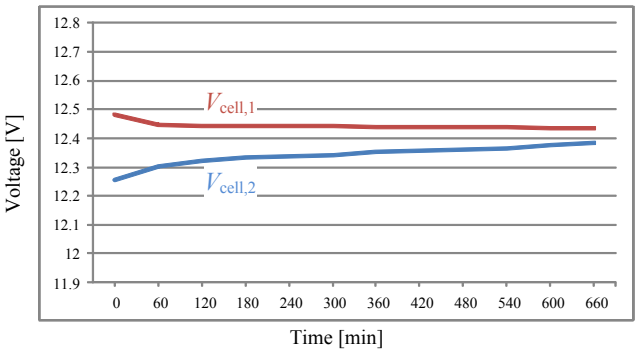

Fig. 11. Experimental results of voltage convergence with two Lead-Acid batteries as cells with different initial voltages.

[13] F. Mestrallet, L. Kerachev, J. C. Crebier and A. Collet, "Multiphase interleaved converter for lithium battery active balancing," *IEEE Trans. Power Electron.*, vol. 29, no. 6, pp. 2874-2881, Jun. 2014.

[14] L. Wang, L. Wang, C. Liao, and J. Liu, "Research on battery balance system applied on HEV," *VPPC '09*, pp. 1788-1791, Sep. 2009.

[15] Z. Nie and C. Mi, "Fast battery equalization with isolated bidirectional DC-DC converter for PHEV applications," *IEEE Vehicle Power and Propulsion Conference, VPPC '08*, pp. 78-81, Sep. 2009.

[16] Y. S. Lee and G. T. Cheng, "Quasi-resonant zero-current-switching bidirectional converter for battery equalization applications," *IEEE Trans. Power Electron.*, vol. 21, no. 5, pp. 1213-1224, Sep. 2006.

[17] M. Uno and K. Tanaka , "Single-switch cell voltage equalizer using multistacked buck-boost converters operating in discontinuous conduction mode for series-connected energy storage cells," *IEEE Trans. Vehicular Technology*, vol. 60, no. 8, pp. 3635-3645, Oct. 2011.

[18] M. Uno and K. Tanaka, "Single-switch multi-output charger using voltage multiplier for series-connected lithium-ion battery/supercapacitor equalization," *IEEE Trans. Ind. Electron.,* vol. 60, no. 8, pp. 3227–3239, Aug. 2013.

[19] G. Oriti, A. L. Julian and P. Norgaard, "Battery management system with cell equalizer for multi-cell battery packs" in *Proc. IEEE Energy Convers. Congr. Expo. 2014*, pp. 900-905, Sep. 2014.

[20] M. Uno and K. Tanaka, "Single-switch cell voltage equalizer using voltage multipliers for series-connected supercapacitors," in *Proc. IEEE Appl. Power Electron. Conf. Expo*, pp. 1266-1272, Feb. 2012.

[21] Y. Yuanmao, K. W. E. Cheng, and Y. P. B. Yeung, "Zero-current switching switched-capacitor zero-voltage-gap automatic equalization system for series battery string", *IEEE Trans. Power Electron.*, vol. 27, no. 7, pp. 3234-3242, Jul. 2012.

[22] C. H. Sung, K. Lee, and B. Kang, "Voltage equalizer for li-ion battery string using LC series resonance," *IECON 2013 - 39th Annual Conference of the IEEE*, pp.1404-1409, Nov. 2013.

[23] A. L. Julian, G. Oriti, M. E. Pfender, "SLR converter design for multi-cell battery charging," in *Proc. IEEE Energy Convers. Congr. Expo.*, pp. 743-748, Sep. 2013.

[24] D. Costinett, K. Hathaway, M. U. Rehman, M. Evzelman, R. Zane., Y. Levron, and D. Maksimovic, "Active balancing system for electric vehicles with incorporated low voltage bus," in *Proc. IEEE Appl. Power Electron. Conf. Expo. 2014*, pp. 3230-3236, Mar. 2014.

[25] S. Li, C. C. Mi and M. Zhang, "A high-efficiency active battery-balancing circuit using multiwinding transformer," *IEEE Trans. Ind. Applications*, vol. 49, no. 1, pp. 198-207, Jan. 2013.

[26] S. H. Park, K. B. Park, H. S. Kim, G. W. Moon, M. J. Youn, "Single-magnetic cell-to-cell charge equalization converter with reduced number of transformer windings," *IEEE Trans. Power Electron.*, vol. 27, no. 6, pp. 2900-2911, Jun. 2012.

[27] M. Y Kim, J. H. Kim, G. W. Moon, "Center-cell concentration structure of a cell-to-cell balancing circuit with a reduced number of switches," *IEEE Trans. Power Electron*., vol. 29, no. 10, pp. 5285–5297, Oct. 2014.

[28] Y. S. Lee and M. W. Cheng, "Intelligent control battery equalization for series connected lithium-ion battery strings," *IEEE Trans. Ind. Electron.*, vol. 52, no. 5, pp. 1297-1307, Oct. 2005.

[29] M. U. Rehman, F. Zhane, M. Evzelman, R. Zane, and D. Maksimovic, "Control of a series-input, parallel-output cell balancing system for electric vehicle battery packs", *IEEE 16th Workshop on Control and Modeling for Power Electronics 2015*, Jul. 2015.

[30] B. Dong, Y. Li and Y. Han, "Parallel architecture for battery charge equalization," *IEEE Trans. Power Electron*., vol. 30, no. 9, pp. 4906-4913, Sep. 2015.

[31] H. S. Park, C. H. Kim; K. B. Park, G. W. Moon and J. H. Lee, "Design of a charge equalizer based on battery modularization," *IEEE Trans. Vehicular Technology*, vol. 58, no. 7, pp. 3216-3223, Sep. 2009.

[32] H. S. Park, C. E. Kim, C. H. Kim, G. W. Moon and J. H. Lee, "A modularized charge equalizer for an HEV lithium-ion battery string," *IEEE Trans. Ind. Electron.*, vol. 56, no. 5, pp. 1464-1476, May 2009.

[33] C. H. Kim, M. Y. Kim, and G. W. Moon, "A modularized charge equalizer using a battery monitoring IC for series-connected Li-ion battery strings in electric vehicles," *IEEE Trans. Power Electron*., vol. 28, no. 8, pp. 3779–3787, Aug. 2013.

[34] M. U. Rehman, M. Evzelman, K. Hathaway, R. Zane, G. L. Plett, K. Smith, E. Wood, and D. Maksimovic, "Modular approach for continuous cell-level balancing to improve performance of large battery packs", ," in *Proc. IEEE Energy Convers. Congr. Expo 2014*, pp. 4327-4334, Sep. 2014.

[35] E. Hamo, M. Evzelman, M. M. Peretz, "Modeling and analysis of resonant switched-capacitor converters with dree-wheeling ZCS," *IEEE Trans. Power Electron*., vol. 30, no. 9, pp. 4952–4959, Sep. 2015.

[36] C. M. T. McLyman, "Winding capacitance and leakage inductance", Chap. 17, *Transformer and Inductor Design Handbook*, 3rd Ed. NY, Marcel Dekker, 2004.